



**Role of chiral-induced spin selectivity in the radical pair mechanism of avian magnetoreception**Yash Tiwari  and Vishvendra Singh Poonia <sup>\*</sup>*Department of Electronics and Communication, Indian Institute of Technology, Roorkee, Uttarakhand 247667, India*

(Received 31 August 2022; accepted 11 December 2022; published 28 December 2022)

In this paper, we investigate the effect of chiral-induced spin selectivity (CISS) on the radical pair mechanism of avian magnetoreception. We examine the impact of spin selectivity on the avian compass sensitivity. In this analysis, we also consider the dipolar and exchange interactions and observe their interplay with CISS. We find that CISS results in a multifold increase in avian compass sensitivity. Interestingly, we also observe that CISS can counter the deleterious effect of dipolar interaction and increase system sensitivity. The analysis has been performed for the toy model (only one nucleus) and a more general case where we consider up to six nuclei from the cryptochrome radical pair system. We observe that the CISS allows the radical pair model to have more realistic recombination rates with good sensitivity. We also do an analysis of the functional window of the avian compass reported in behavioral experiments in the functional window. We could not find a parameter set where a functional window can be observed along with CISS. We also show the effect of spin relaxation on the system and show that under relaxation, CISS shows increased compass sensitivity compared to no CISS case.

DOI: [10.1103/PhysRevE.106.064409](https://doi.org/10.1103/PhysRevE.106.064409)**I. INTRODUCTION**

The avian magnetoreception is the ability of migratory birds to sense the geomagnetic field and navigate with its assistance. Two alternative theories are proposed to understand avian magnetoreception. One is based on magnetite [1,2] and the other on the radical pair model [3], with evidence strongly favoring the later [3–5].

The radical pair model (RPM) is based on the spin of two electrons created on adjacent radicals (donor and acceptor). The formation of this radical pair is attributed to the photoexcitation of the donor and acceptor molecules, whereby an electron transfer is involved. The photoexcitation happens due to light of a particular frequency falling on the bird's retina, which is the site of these donor and acceptor molecules. The spin of these two electrons interacts with the earth's magnetic field and hyperfine field due to surrounding nuclei. In addition, there is electron-electron interaction in the form of dipolar and exchange interactions. All these interactions affect the final entity that is obtained after recombination. Evidences suggest that the donor and acceptor molecules are cofactors of a cryptochrome molecule [3,6–11].

However, an important aspect often disregarded is the electron transfer medium and how it might affect the system. The electron transfer between donor and acceptor essentially happens in a chiral medium. And, according to the chiral-induced spin selectivity (CISS) effect, electron transport in a chiral medium is spin selective [12], which illustrates that chiral molecules act as a spin filter and a certain chirality only allows electrons of a particular spin to travel through it [13–15]. The reason attributed to this spin selective assistance is the spin-orbit interaction, which effectively interacts

with the linear momentum of the electron. The electrostatic potential provided by the chiral molecules' geometric structure accelerates the electron's momentum having a particular kind of spin [16–18]. Recently, Luo and Hore analyzed the RPM of the avian compass with CISS [19]. This calls for a more comprehensive analysis of the effect of CISS on the radical pair spin dynamics and various behavioral characteristics of the avian compass.

In this paper, our focus is to understand the interplay between CISS and various parameters of the RPM of the avian compass, and we analyze the functional window characteristics of the avian compass in the light of CISS. The functional window is the behavioral characteristics of the compass that refers to the selectivity of the compass around the geomagnetic fields ( $25 \mu\text{T}$  to  $65 \mu\text{T}$ ) [20–24]. This is an important yet not well-understood feature of the avian compass, especially from the point of view of the RPM. We study the effect of CISS for various recombination rates of radicals. Additionally, dipolar and exchange interactions are usually detrimental to the action of the avian compass and cause a reduction in the compass sensitivity. However, it was observed that exchange and dipolar interaction could partially cancel each other, thereby restoring the sensitivity to some extent [25]. It becomes important to observe how electron-electron interaction affects sensitivity in conjunction with CISS. We also examine the effect of decoherence on the system and show that CISS protects the sensitivity of the compass under decoherence. We first analyze the effect of CISS on system yield, sensitivity, and functional window for a radical pair toy model (where only one nucleus is considered) and a realistic cryptochrome-based radical pair system where we consider two nuclei each on flavin adenine dinucleotide FAD (two nitrogen nuclei) and tryptophan TrpH (one nitrogen and one hydrogen) radicals. The FAD act as a donor entity, whereas TrpH act as an acceptor entity. Then, we observe

<sup>\*</sup>vishvendra@ece.iitr.ac.in

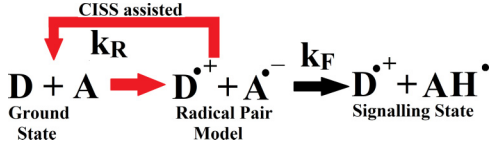


FIG. 1. Schematic of the radical pair mechanism with chiral-induced spin selectivity (CISS) where  $D$  denotes the donor molecule and  $A$  represents the acceptor molecule. The red back-arrow denotes the CISS-assisted recombination to the ground state.

the effect of dipolar and exchange interaction on the CISS-assisted magnetoreception. This is followed by the effect of decoherence on the sensitivity of the compass for various values of CISS.

The paper has been organized as follows: Section II discusses the simulation methodology followed for analysis. Section III discusses the results, where Sec. III A discusses the effect of CISS on sensitivity, Sec. III B discusses the effect of CISS on the functional window, and Sec. III C explores the impact of electron-electron interaction system sensitivity along with CISS. Section IV explores the effect of decoherence on CISS-assisted avian magnetoreception.

## II. METHODOLOGY

We study the cryptochrome (four nuclei)-based RPM of an avian compass [9,26,27].

In this model, photoexcitation of the acceptor molecule leads the electron from a ground to excited state, leaving a vacancy in the ground state. An adjacent donor molecule donates an electron to fill the vacancy in the ground state of the acceptor. Hence a radical pair is formed: one unpaired electron in the ground state of the donor (spin operator  $S_D$ ) and the other unpaired electron in the excited state of the acceptor (spin operator  $S_A$ ). The radical pair recombines back to form the ground state of the system or forms a signaling state after protonation of the acceptor molecule. The schematic of this mechanism is given in Fig. 1. We account for CISS in the formation of radical pair as a result of electron transfer from donor to acceptor and in formation of ground state due to reverse electron transfer. However, formation of signaling state from the radical pair does not involve any electron transfer; therefore, CISS does not play any role in this leg of RPM.

The spin selectivity of the system due to CISS (shown by red arrow in Fig. 1) is captured by the initial state and the ground state formed after recombination. This model is discussed in more detail in Ref. [19].

The spin state of the radical pair can be a singlet state, triplet state, or a superposition thereof. The spin dynamics is governed by the Hamiltonian [19,28,29]:

$$\hat{H} = \omega \cdot (\hat{S}_A + \hat{S}_D) + \sum_{i \in D,A} \sum_k \hat{S}_i \cdot A_{ik} \cdot \hat{J}_{ik} - J(2\hat{S}_A \cdot \hat{S}_D + 0.5) + \hat{S}_A \cdot D \cdot \hat{S}_B. \quad (1)$$

$\hat{S}_A$  and  $\hat{S}_D$  are spin of electron on donor and acceptor molecule,  $\omega = g\mu_B \bar{B}$ , where  $\bar{B} = B_0((\cos\theta \cos\phi)\bar{x} + (\cos\theta \sin\phi)\bar{y} + (\cos\theta)\bar{z})$ .  $B_0$  corresponds to the earth's magnetic field, which in our works is assumed to

be  $50 \mu\text{T}$ .  $\theta$  and  $\phi$  describe orientation of magnetic field with respect to hyperfine tensor [30].  $J$  is the electron-electron spin-exchange interaction, whereas  $D$  is the dipole-dipole interaction tensor. The form of dipolar Hamiltonian depends upon the relative direction of electron spin with each other and the externally applied magnetic field.  $A_{ik}$  is the hyperfine interaction between electron and nuclear spin  $x, y, z$  components.

The initial density of matrix of the system is given by  $P_I = |\psi_I\rangle \langle \psi_I| \otimes \frac{1}{Z}$ , where  $\frac{1}{Z}$  corresponds to the normalized mixed state of the nuclei ( $Z$  is sized of combined Hilbert space of nuclei).  $|\psi_I\rangle$  is the initial state of the radical pair. If the CISS-assisted recombination back to the ground state is represented by  $|\psi_R\rangle$ , then

$$|\psi_I\rangle = \frac{1}{\sqrt{2}}[\sin(0.5\chi) + \cos(0.5\chi)]|\uparrow_D \downarrow_A\rangle + \frac{1}{\sqrt{2}}[\sin(0.5\chi) - \cos(0.5\chi)]|\downarrow_D \uparrow_A\rangle, \quad (2)$$

$$|\psi_R\rangle = -\frac{1}{\sqrt{2}}[\sin(0.5\chi) - \cos(0.5\chi)]|\uparrow_D \downarrow_A\rangle - \frac{1}{\sqrt{2}}[\sin(0.5\chi) + \cos(0.5\chi)]|\downarrow_D \uparrow_A\rangle. \quad (3)$$

The parameter  $\chi \in [0, \frac{\pi}{2}]$  depends on the spin selectivity of the medium in which the reaction is taking place. When  $\chi = 0$ ,  $|\psi_I\rangle = \frac{1}{\sqrt{2}}|\uparrow_D \downarrow_A\rangle - |\downarrow_D \uparrow_A\rangle$ , and  $|\psi_R\rangle = \frac{1}{\sqrt{2}}|\uparrow_D \downarrow_A\rangle - |\downarrow_D \uparrow_A\rangle$  but when  $\chi = \frac{\pi}{2}$ ,  $|\psi_I\rangle = |\uparrow_D \downarrow_A\rangle$ , and  $|\psi_R\rangle = |\downarrow_D \uparrow_A\rangle$ . These depict the two extremes of the CISS of the chiral medium.  $\chi = 0$  denotes the case with no CISS in the medium (conventional RPM), whereas  $\chi = \frac{\pi}{2}$  signifies the case when the medium is fully chiral (100% CISS).  $0 < \chi < \pi/2$  represents an intermediate and more realistic case. Figure 1 depicts the CISS assisted chemical reaction where  $k_R$  is the rate of recombination of radical back to ground state.  $k_F$  is rate at which the radical pair protonate with  $H^+$  to create the signaling state:

$$\frac{d\hat{\rho}}{dt} = -(\text{coh} + \text{recomb}) - i[\hat{H}, \hat{\rho}(t)] - \frac{1}{2}k_R[|\psi_R\rangle \langle \psi_R|, \hat{\rho}(t)] - k_F \hat{\rho}(t). \quad (4)$$

The master equation governing the system is given by Eq. (4), where coh corresponds to the coherent evolution of the system and recomb corresponds to the chemical dissipation responsible for the formation of yield product which enables birds to do magnetoreception. In Liouville space, this is accomplished by using a projection operator, which maps the yield of the system into the shelving states as done in Refs. [30,31].

## III. RESULTS AND DISCUSSION

This section is divided into three subsections. In the first two subsections, we report the effect of CISS on sensitivity and functional window in the absence of electron-electron interactions (exchange and dipolar interactions). In the last subsection, we also include dipolar and exchange interactions in CISS framework and observe the sensitivity of the compass.

### A. Effect of CISS on sensitivity

To define the sensitivity of the avian compass, the yield product of either the signaling state ( $\phi_F$ ) or ground state ( $\phi_R$ ) needs to be defined. The yield of the signaling state ( $\phi_F$ ) is defined by Eq. (5), where  $\rho(t)$  is the solution of the master equation, Eq. (4),  $\text{Tr}$  is the trace over the state density matrix  $\rho$ .  $k_F$  is the rate associated with the signaling state. The yield of the ground state ( $\phi_R$ ) associated with recombination operator  $|\psi_R\rangle\langle\psi_R|$  can easily be found by  $\phi_R + \phi_F = 1$ . We use the semiclassical formalism of Eq. (5) to avoid solving in Liouville space, which poses a significant computation challenge. The formalism has been initially proposed in Ref. [32] and reiterated in Ref. [33]

$$\phi_F = k_F \int_0^\infty P_S(t) dt = k_F \int_0^\infty \text{Tr}[\rho(t)] dt, \quad (5)$$

$$\Delta\phi_R = \max_{\theta, \phi}(\phi_R) - \min_{\theta, \phi}(\phi_R). \quad (6)$$

The sensitivity of the avian compass is defined in Eq. (6). The difference between the maximum and minimum  $\phi_R$  is taken over all the values of  $\phi$  and  $\theta$ . A measure of sensitivity can be either  $\Delta\phi_R$  or  $\Delta\phi_F$ . In our paper, we choose  $\Delta\phi_R$  to describe the sensitivity. Sensitivity quantifies the yield range for the same  $\theta$  and  $\phi$ , which essentially describes the longitudinal and latitudinal position on earth. We ideally require this sensitivity to be as high as possible for better operation of the avian compass. We also define a quantity which will help us quantify the change in sensitivity due to CISS:

$$\Delta M_S = \frac{\Delta\phi_R(\chi = \frac{\pi}{2})}{\Delta\phi_R(\chi = 0)}. \quad (7)$$

The toy model we consider consists of two electrons and a single nucleus. One electron interacts with the nucleus having spin  $\frac{1}{2}$ . The cryptochrome (four nuclei) system is modeled with each electron having hyperfine interaction with two nuclei. Figure 2 shows the product yield of the ground state ( $\phi_R$ ) as a function of  $\theta$  for varying degrees of spin selectivity due to CISS. Each color corresponds to the product yield at a single value of  $\chi$  depicting a certain degree of spin selectivity for  $\phi = 0$  and  $\theta \in \{0^\circ, 180^\circ\}$ . Figures 2(a) and 2(b) correspond to  $\phi_R$  versus  $\theta$  when  $(k_F, k_R) = (10^6, 10^6) s^{-1}$  and  $(k_F, k_R) = (10^6, 10^8) s^{-1}$ , respectively, for the toy model. Figures 2(c) and 2(d) correspond to case  $(k_F, k_R) = (10^6, 10^6) s^{-1}$  and  $(k_F, k_R) = (10^6, 10^8) s^{-1}$ , respectively, for the realistic case of cryptochrome (four nuclei)-based RP system. The reaction rate  $(k_F, k_R) = (10^6, 10^8) s^{-1}$  is the most realistic recombination rate set in the RPM as it indicates that the rate of protonation is slower than back recombination. We observe from Fig. 2 that the yield plot is symmetric about  $\theta = 90^\circ$  when  $\chi = 0$ , but such is not the case when  $\chi = \frac{\pi}{2}$ . Hence, we lose symmetry of the yield with respect to  $\theta$  due to CISS. Interestingly, we also observe that  $\Delta\phi_R$  is dramatically increased for  $\chi = \frac{\pi}{2}$  case in Fig. 2(b) compared to  $\chi = 0$ .  $\Delta\phi_R$  is comparable for both of these extreme cases in Fig. 2(a). We observe this for a single  $\phi = 0$ , assuring us that the minimum value of  $\Delta\phi_R$  is quite high for CISS-assisted avian magnetoreception into the toy model. A similar observation is made for the four-nuclei RP case also. From Fig. 2, we observe that for  $(k_F, k_R) = (10^6, 10^6) s^{-1}$ , the sensitivity

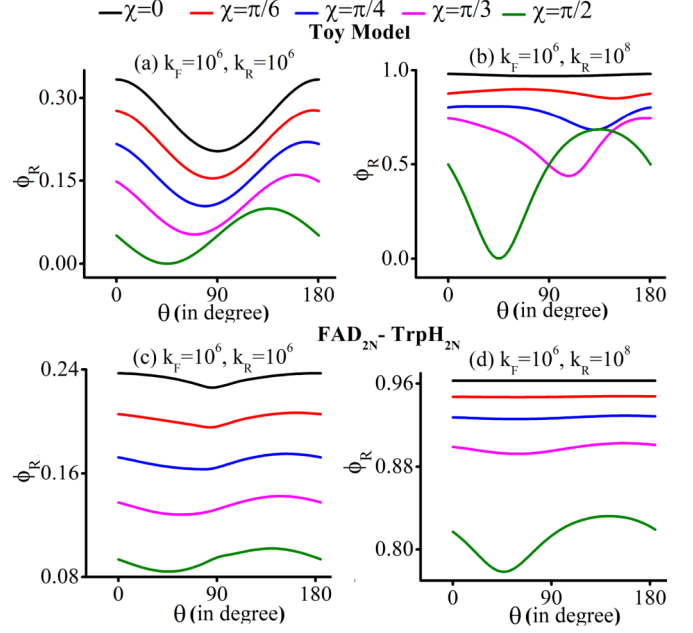


FIG. 2. Yield of the ground state ( $\phi_R$ ) versus  $\theta$  for constant  $\phi(=0)$  for five distinct values of  $\chi$  (showing the varying degrees of spin selectivity due to CISS;  $0^\circ$ —black,  $30^\circ$ —red,  $45^\circ$ —blue,  $60^\circ$ —pink,  $90^\circ$ —green). The result is shown at two values of signaling state recombination rate ( $k_F$ ) and ground-state recombination rate ( $k_R$ ), i.e., (a)  $(k_F, k_R) = (10^6, 10^6) s^{-1}$ , (b)  $(k_F, k_R) = (10^6, 10^8) s^{-1}$ . (a) and (b) in the top row show the yield for a toy model at the two specified rates for various values of  $\chi$ . (c) and (d) in the bottom row show the yield for the specified cryptochrome-based four-nuclei RP ( $\text{FAD}_{2N}^* - \text{TrpH}_{2N}^*$ ) system at the two rates for various values of  $\chi$ .

remains more or less the same as we increase CISS, but the yield of the ground state decreases (signaling state yield increases). For  $(k_F, k_R) = (10^6, 10^8) s^{-1}$ , we observe an increase in sensitivity with CISS; however, an increase of signaling state yield is observed with CISS. This was observed for both the toy model and the four-nuclei model for the cryptochrome system. We have given contour plots for the toy model and four-nuclei cryptochrome system in Appendix A, depicting  $\Delta\phi_R$  for various values of  $k_F, k_R$ . We conclude that the range of  $k_F, k_R$  in the toy model is broader as compared to the four-nuclei case. In Table I, we summarize the value of  $\Delta M_S$  at given rate combinations for a four-nuclei system. In Table II, we summarize  $\Delta M_S$  values for six nuclei-based cryptochrome systems.

TABLE I.  $\Delta M_S$  for cryptochrome-based radical pair model ( $\text{FAD}_{2N}^* - \text{TrpH}_{2N}^*$ ) with four nuclei for various rate combination at  $D = 0$  and  $J = 0$ .

$k_R \downarrow, k_F \rightarrow$	$10^4 s^{-1}$	$10^5 s^{-1}$	$10^6 s^{-1}$	$10^7 s^{-1}$	$10^8 s^{-1}$
$10^4 s^{-1}$	1.12	0.72	1.27	2.03	2.25
$10^5 s^{-1}$	5.78	1.09	1.34	2.04	2.25
$10^6 s^{-1}$	219.02	8.46	1.37	2.14	2.25
$10^7 s^{-1}$	1.17E + 04	409.54	16.09	3.25	2.32
$10^8 s^{-1}$	1.41E + 05	1.06E + 04	68.84	30.27	3.14

TABLE II.  $\Delta M_S$  for cryptochrome-based radical pair model ( $\text{FAD}_{3N}^{\bullet} - \text{TrpH}_{3N}^{\bullet}$ ) with six nuclei for various rate combination at  $D = 0$  and  $J = 0$ .

$k_R \downarrow, k_F \rightarrow$	$10^4 \text{ s}^{-1}$	$10^5 \text{ s}^{-1}$	$10^6 \text{ s}^{-1}$	$10^7 \text{ s}^{-1}$	$10^8 \text{ s}^{-1}$
$10^4 \text{ s}^{-1}$	1.52	6.86	0.55	1.67	0.49
$10^5 \text{ s}^{-1}$	6.86	1.20	0.86	0.99	1.97
$10^6 \text{ s}^{-1}$	87.95	6.399	1.05	1.06	1.98
$10^7 \text{ s}^{-1}$	1.32E+03	132.73	11.13	1.85	2.07
$10^8 \text{ s}^{-1}$	2.50E+04	2.43E+03	52.97	13.71	2.97

We found  $\Delta M_S$  greater than unity for certain rate combinations even for the six nuclei case, which ascertains CISS assisted sensitivity enhancement even with six nuclei, especially with realistic recombination rate sets, i.e.,  $(k_F, k_R)$  close to  $(10^6, 10^8)$ . As expected, we find a reduction of  $\Delta M_S$  values as the number of nuclei increases. This leads to the question whether the positive effect of CISS will be sustained in a real cryptochrome system.

### B. Effect of CISS on functional window

The functional window is the selectivity of the avian compass with respect to the external magnetic field. It can be studied by analyzing sensitivity ( $\Delta\phi_R$ ) as a function of the magnetic field—the system with respect to the external magnetic field. Based on the behavioral experiment, we expect that the avian compass shows maximum sensitivity around the earth's magnetic field and a reduced sensitivity around other magnetic fields [3,22].

We plot the functional window in Fig. 3 for the toy model and in Fig. 4 for the cryptochrome-based RP system. We plot  $\Delta\phi_R$  as a function of the external magnetic field. In Fig. 3(a), we plot the  $\Delta\phi_R$  for  $k_F = 10^4 \text{ s}^{-1}$  and  $k_R \in \{10^4, 10^5, 10^6, 10^7, 10^8, 10^9\} \text{ s}^{-1}$

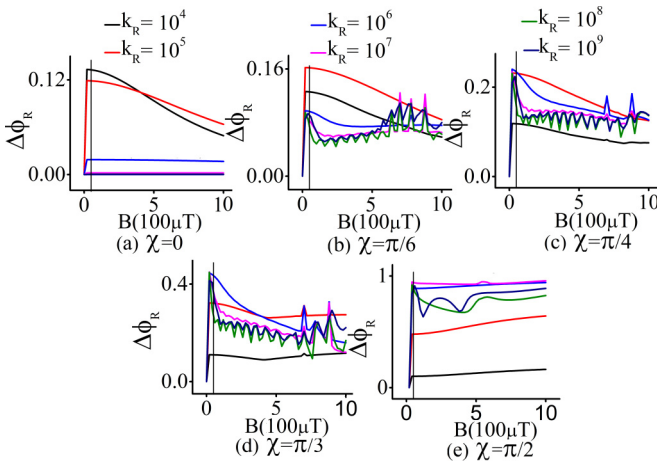


FIG. 3. Sensitivity ( $\Delta\phi_R$ ) versus  $B(\times 100 \mu T)$  for five distinct values of  $\chi$  showing varying degrees of spin selectivity due to CISS ( $0^\circ, 30^\circ, 45^\circ, 60^\circ, 90^\circ$ ). This calculation is shown for  $k_F = 10^4 \text{ s}^{-1}$  and  $k_R \in \{10^4, 10^5, 10^6, 10^7, 10^8, 10^9\} \text{ s}^{-1}$ . The vertical line marked in each figure corresponds to  $B = 50 \mu T$ .

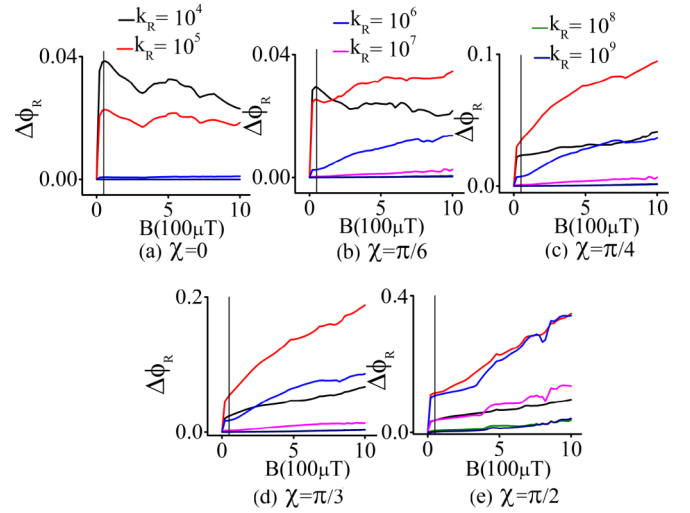


FIG. 4. Sensitivity ( $\Delta\phi_R$ ) versus  $B(\times 100 \mu T)$  for five distinct values of  $\chi$  showing varying degrees of spin selectivity due to CISS ( $0^\circ, 30^\circ, 45^\circ, 60^\circ, 90^\circ$ ). The calculation is shown for  $k_F = 10^4 \text{ s}^{-1}$  and  $k_R \in \{10^4, 10^5, 10^6, 10^7, 10^8, 10^9\} \text{ s}^{-1}$  and realistic cryptochrome-based RP system. The vertical line marked in each figure corresponds to  $B = 50 \mu T$ .

We observe that sensitivity increases with the channel's spin selectivity  $\chi$ . For the toy model, the functional window is preserved even with CISS; however, the rate combination at which CISS shows maximum sensitivity and selectivity varies. We observe that the system is showing at CISS  $\chi = \frac{\pi}{3}$  for rate combination  $(k_F, k_R) = (10^4, 10^6) \text{ s}^{-1}$  maximum sensitivity with the functional window feature preserved. At  $\chi = \frac{\pi}{2}$ , a window is observed to a certain degree for combination  $(k_F, k_R) = (10^4, 10^8) \text{ s}^{-1}$  and  $(k_F, k_R) = (10^4, 10^9) \text{ s}^{-1}$ , but these values of  $k_R$  seem unrealistic based on the timescales of RPM as we know.

For the realistic case (Fig. 4), in the functional window, we observe that for the  $\chi = 0$  case, compass selectivity or window is maintained. The introduction of CISS in the avian compass model loses its functional window feature and shows an increase in sensitivity at higher magnetic field values. This is not in agreement with behavioral experiments performed on the avian compass [3,20,22,23]. Thus, the functional window could not be modeled even in CISS despite an increase in compass sensitivity. This is, in general, agreement with previous results where the functional window is not visible at high recombination rates [21]. We are further exploring the CISS-based model to see if it can exhibit a functional window for some set of compass parameters.

### C. Effect of electron-electron interactions

So far, we have not included the effect of electron-electron interactions. In this section, we examine the effect of dipolar and exchange interactions along with CISS on compass sensitivity. Both of these effects arise due to the spin property of the electrons.

Dipolar interaction ( $D$ ) is proportional to  $r^{-3}$  as given in Eq. (8) whereas exchange interaction ( $J$ ) is proportional to

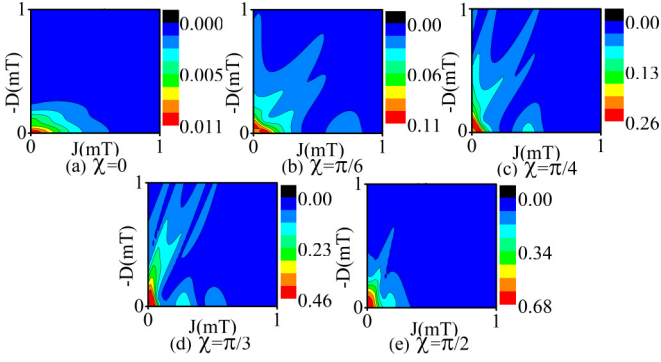


FIG. 5. Plots for sensitivity  $\Delta\phi_R$  as a function of  $D$ (mT) and  $J$ (mT) for five distinct values of  $\chi$  showing varying degrees of spin selectivity due to CISS ( $0^\circ$ ,  $30^\circ$ ,  $45^\circ$ ,  $60^\circ$ ,  $90^\circ$ ) at  $(k_F, k_R) = (10^6, 10^8) s^{-1}$  for toy model.

$e^{-r}$  as given in Eq. (9) [25], where  $r$  is the distance between the two electrons:

$$D(r) = -\frac{3}{2} \frac{\mu_o \gamma_e^2 \hbar^2}{4\pi r^3} \Rightarrow D(r)/\mu T = -\frac{2.78 \times 10^3}{(r/\text{nm})^3}, \quad (8)$$

$$J(r) = J_0 e^{-\beta r}. \quad (9)$$

When the distance between the two spin  $r > 1.9$  nm, we assume in the avian compass that the dipolar Hamiltonian is dominant and the exchange interaction can be neglected [25]. In Eq. (9),  $J_0$  and  $\beta$  are empirical parameters [34,35].

Henceforth, we take the realistic set of rates  $[(k_F, k_R) = (10^6, 10^8) s^{-1}]$  in our analysis. We analyze the contour plots of sensitivity as a function of  $D$  and  $J$  for five distinct values of  $\chi$  (CISS) ( $0^\circ$ ,  $30^\circ$ ,  $45^\circ$ ,  $60^\circ$ ,  $90^\circ$ ). Figure 5 presents the sensitivity contours for the toy model. In these plots, the dipolar interaction value is taken from  $-1$  mT to 0; similarly, the exchange interaction value is considered from 0 to 1 mT. For the contour plots,  $\Delta\phi_R$  is calculated for  $(k_F, k_R) = (10^6, 10^8) s^{-1}$ .

In Fig. 5, for  $\chi = 0$  (no CISS), we observe that compass sensitivity is notable for exchange interaction ( $J$ ) from 0 to  $\sim 0.5$  mT and dipolar interaction ( $D$ ) from 0 to about  $\sim -0.2$  mT. As observed in previous results as well, the compass sensitivity increases significantly when CISS is considered (nonzero  $\chi$ ). Interestingly, we observe that for  $\chi = \frac{\pi}{6}$ ,  $\frac{\pi}{4}$ , and  $\frac{\pi}{3}$  the compass sensitivity  $\Delta\phi_R$  at  $D=0.1$  mT is greater than that at  $D=0$  mT for  $J=0$  mT. This is further confirmed in Fig. 6 where the compass sensitivity ( $\Delta\phi_R$ ) is plotted with respect to  $\chi$  for five values of dipolar interaction at  $J=0$ ; This is done for two rates at  $(k_F, k_R) = (10^6, 10^6) s^{-1}$  [Fig. 6(a)] and  $(k_F, k_R) = (10^6, 10^8) s^{-1}$  [Fig. 6(b)]. We observe in Fig. 6(b) that for a certain value of  $\chi$ , it is not necessary that a higher value of dipolar interaction results in a low value of sensitivity  $\Delta\phi_R$ . In other words, CISS is canceling the effect of dipolar interaction for some degrees of spin selectivity.

To get a more realistic picture, we similarly analyze the cryptochrome-based four-nuclei RP system. In Fig. 7, we plot the compass sensitivity as a function of  $\chi$  for five distinct values of dipolar interaction ( $D$ ). Figures 7(a) and 7(b) correspond to the plots for  $(k_F, k_R) = (10^6, 10^6) s^{-1}$  and  $(k_F, k_R) = (10^6, 10^8) s^{-1}$  respectively. In the bottom row, we have enlarged region (A) of Fig. 7(b) for  $(k_F, k_R) = (10^6, 10^8) s^{-1}$

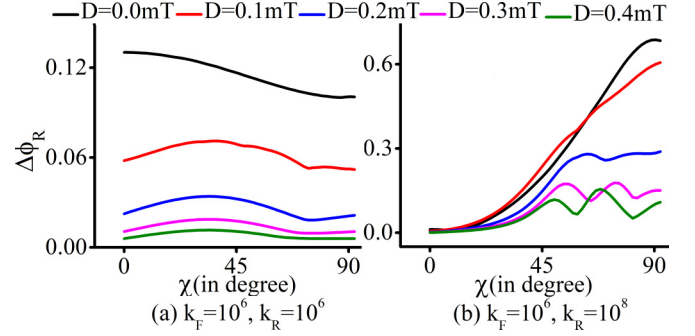


FIG. 6. Sensitivity ( $\Delta\phi_R$ ) versus  $\chi$  for two combinations of signaling state rate ( $k_F$ ) and ground-state recombination rate ( $k_R$ ), i.e., (a)  $(k_F, k_R) = (10^6, 10^6) s^{-1}$ , (b)  $(k_F, k_R) = (10^6, 10^8) s^{-1}$  for five values of dipolar interaction ( $D$ ) when  $J=0$ .

in Fig. 7(c), region (B) of Fig. 7(c) is further enlarged. We observe that a higher value of  $D$  does not necessarily mean a lower sensitivity value in a chiral medium. We observe from Fig. 7(c) that for  $\chi \leq 50^\circ$ , the sensitivity is higher in the presence of dipolar interaction due to CISS.

Further, we analyze the effect of exchange interaction in conjunction with dipolar interaction along with CISS for the four-nuclei RP system, as done earlier for the toy model in Fig. 5. In Fig. 8, we plot the compass sensitivity ( $\Delta\phi_R$ ) as function of  $D$  and  $J$  at rate  $(k_F, k_R) = (10^6, 10^8) s^{-1}$  for five distinct values of  $\chi$  ( $0^\circ$ ,  $30^\circ$ ,  $45^\circ$ ,  $60^\circ$ ,  $90^\circ$ ).

We found that chirality affects the dipolar and exchange value for which we attain the maxima of compass sensitivity. When  $\chi=0$ , we observe that maximum sensitivity is no longer at  $J=0$  and  $D=0$ . We observe the compass sensitivity max-

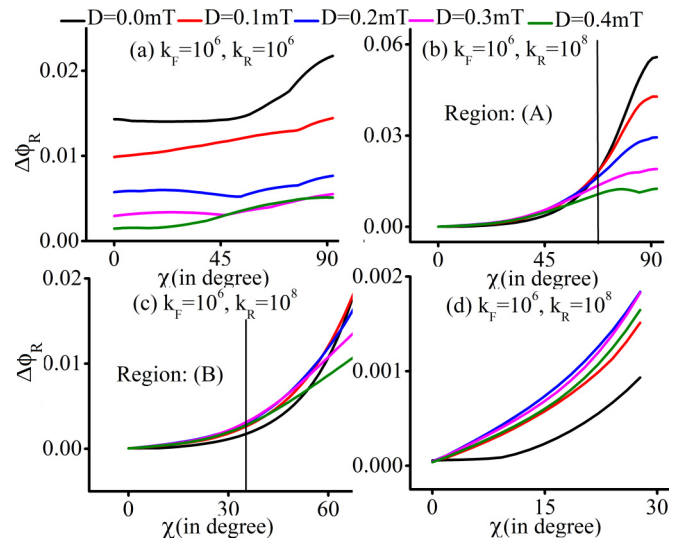


FIG. 7. Top: Sensitivity ( $\Delta\phi_R$ ) versus  $\chi$  for two combinations of signaling state rate ( $k_F$ ) and ground-state rate ( $k_R$ ), i.e., (a)  $(k_F, k_R) = (10^6, 10^6) s^{-1}$ , (b)  $(k_F, k_R) = (10^6, 10^8) s^{-1}$  for cryptochrome-based four nuclei RP system. In (b), region (A) has been enlarged in the bottom pane. Bottom: (c) Region (A) is enlarged, and in (d) Region (B) of (c) has been enlarged, showing values of  $\chi$  for which  $\Delta\phi_R$  at zero dipolar interaction ( $D=0$ ) is smaller than the case when dipolar interaction is nonzero.

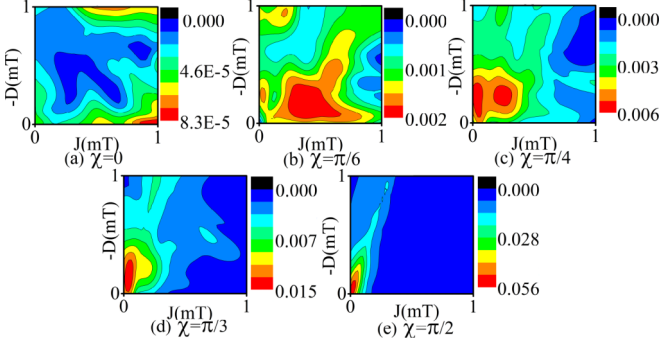


FIG. 8. Plots for sensitivity ( $\Delta\phi_R$ ) as a function of  $D$ (mT) and  $J$ (mT) for five distinct values of  $\chi$  showing varying degrees of spin selectivity due to CISS ( $0^\circ$ ,  $30^\circ$ ,  $45^\circ$ ,  $60^\circ$ ,  $90^\circ$ ) at  $(k_F, k_R) = (10^6, 10^8) s^{-1}$  for four-nuclei  $FAD_{2N}^* - TrpH_{2N}^*$  based RP system.

ima in region where  $J \neq 0, D \neq 0$  for  $\chi = \frac{\pi}{6}$  and  $\chi = \frac{\pi}{4}$ . This region shrinks and again converges to the origin ( $J = 0$  and  $D = 0$ ) as  $\chi$  is further increased. Full CISS results in a small range of dipolar and exchange values with compass sensitivity showing maxima near the origin. This confirms our result of Fig. 7, where we showed for  $\chi \leq 50^\circ$  dipolar interaction is required for increased sensitivity. In addition to this, for  $\chi = \frac{\pi}{6}$  and  $\chi = \frac{\pi}{4}$ , we find finite  $J$  also results in increased sensitivity. Thus, CISS cancels the deleterious effect of dipolar and exchange interactions in these regimes. For cases  $\chi = \frac{\pi}{3}$  and  $\chi = \frac{\pi}{2}$ , however, we observe that a lower value of  $D$  and  $J$  corresponds to the increased sensitivity.

Finally, we have provided similar contour plots for the toy model and four-nuclei-based RP system at  $(k_F, k_R) = (10^6, 10^6) s^{-1}$  in the Appendices. There, we observe that we get a lesser range of  $D$  and  $J$  values for which we get significant compass sensitivity in the toy model. For the four-nuclei RP system, we do observe sensitivity rise around  $J \sim 0.4$  mT,  $D \sim 1$  mT when  $\chi = 0$ . An increase in sensitivity was observed with an increase in CISS. A larger range of  $J \in \{0, 0.5$  mT} and  $D \in \{0, 1$  mT} shows us an increase in sensitivity as  $\chi$  increases from 0 to  $\frac{\pi}{2}$ . Hence, in a nutshell, CISS allows us to have sensitivity at higher recombination rates, and at these higher rates, we observe mitigation of detrimental effects of dipolar and exchange interactions to a certain extent.

In our analysis, we have taken two cases of the rate at  $(k_F, k_R) = (10^6, 10^6) s^{-1}$  and  $(k_F, k_R) = (10^6, 10^8) s^{-1}$ . This is done to show the difference between symmetric and asymmetric radical pair recombinations. In a realistic radical pair system, it is improbable that both rates will have the same value. Protonation is generally slower than back recombination to the ground state; hence a realistic case is one with  $(k_F, k_R) = (10^6, 10^8) s^{-1}$ . The range of dipolar and exchange interactions considered is in a realistic range. However, an exact value is difficult to ascertain since the distance between two radicals may change in an aqueous biological medium. The spin selectivity  $\chi$  of the chiral medium will be an intermediate value (between 0 and  $\frac{\pi}{2}$ ). Until the structure of the medium is ascertained, it is difficult to comment on the exact value of  $\chi$ . We observe the highest sensitivity for  $J=0, D=0$ , and  $\chi = \frac{\pi}{2}$  which is an ideal case. Therefore, we have taken a

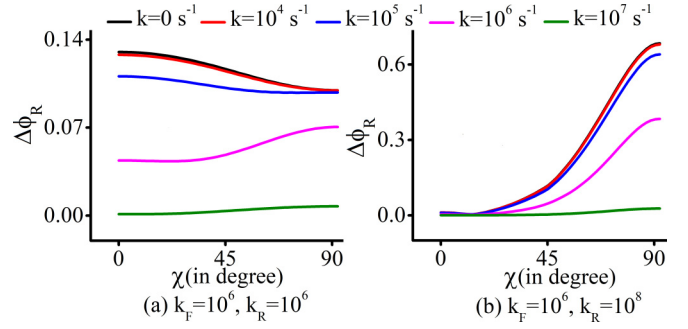


FIG. 9. Sensitivity ( $\Delta\phi_R$ ) versus  $\chi$  for two combinations of signaling state rate ( $k_F$ ) and ground state rate ( $k_R$ ), i.e., (a)  $(k_F, k_R) = (10^6, 10^6) s^{-1}$ , (b)  $(k_F, k_R) = (10^6, 10^8) s^{-1}$  for five values of decoherence rate  $k$ . This result is for the toy model with  $D = 0$  and  $J = 0$ .

range of these realistic values to understand the effect of these parameters on compass sensitivity in a comprehensive way.

#### IV. CISS ALONG WITH ENVIRONMENTAL DECOHERENCE

In this section, we consider the effect of environmental decoherence along with CISS on compass action. We modify Eq. (4) to account for decoherence using Lindblad projection operators:

$$\begin{aligned} \frac{d\hat{\rho}}{dt} &= -(\text{coh} + \text{recomb} + \text{decoh}) \\ &= -i[\hat{H}, \hat{\rho}(t)] - \frac{1}{2}k_R[|\psi_R\rangle\langle\psi_R|, \hat{\rho}(t)] - k_F\hat{\rho}(t) \\ &\quad + k \sum_n \frac{1}{2}\{2C_n\rho(t)C_n^\dagger - \rho(t)C_n^\dagger C_n - C_n^\dagger C_n\rho(t)\}. \end{aligned} \quad (10)$$

Mathematically, we take six spin relaxation operators  $C_1 = \sigma_x \otimes I_{E2} \otimes I_N, C_2 = \sigma_y \otimes I_{E2} \otimes I_N, C_3 = \sigma_z \otimes I_{E2} \otimes I_N, C_4 = I_{E1} \otimes \sigma_x \otimes I_N, C_5 = I_{E1} \otimes \sigma_y \otimes I_N,$  and  $C_6 = I_{E1} \otimes \sigma_z \otimes I_N$  [30].  $I_{E1}$  corresponds to the mixed state of the electron on the radical on FAD molecule, while  $I_{E2}$  corresponds to the mixed state of the electron on the radical on TrpH molecule.  $I_N$  is the combined mixed state of the nuclei and  $k$  is the decoherence rate due to spin relaxation.

In Fig. 9, we plot sensitivity ( $\Delta\phi_R$ ) versus  $\chi$  for five values of relaxation rate  $k$  for the toy model. We observe in Fig. 9(a) that at  $(k_F, k_R) = (10^6, 10^6) s^{-1}$  and  $k = 10^4 s^{-1}, k = 10^5 s^{-1}$  sensitivity changes for  $\chi = 0$  but it does not change for  $\chi = \frac{\pi}{2}$ . At the decoherence rate of  $k = 10^6 s^{-1}$ , we observe that the drop in sensitivity for  $\chi = 0$  is greater than that for  $\chi = \frac{\pi}{2}$ . Hence the sensitivity is more for  $\chi = \frac{\pi}{2}$  than that for  $\chi = 0$ . At  $k = 10^7 s^{-1}$ , sensitivity is negligible for  $\chi = 0$ , but it is nonzero for the full CISS case. In Fig. 9(b), we take  $(k_F, k_R) = (10^6, 10^8) s^{-1}$  with various decoherence rates. We observe that for all values of decoherence rates, the sensitivity for  $\chi = 0$  is less than that for  $\chi = \frac{\pi}{2}$ . It indicates that CISS helps the compass maintain sensitivity even in the presence of environmental decoherence.

In Fig. 10, we plot sensitivity ( $\Delta\phi_R$ ) versus  $\chi$  for five values of decoherence rates  $k$  for a two nuclei-based cryptochrome system. We plot sensitivity in Fig. 10(a)

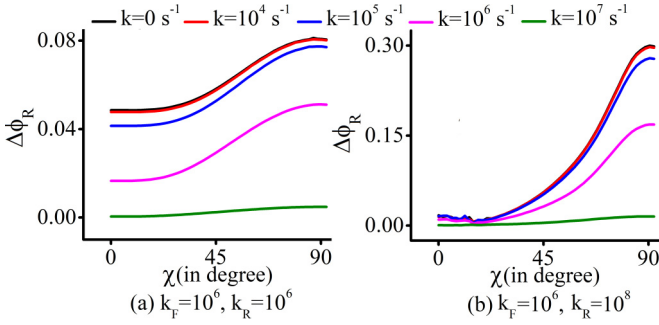


FIG. 10. Sensitivity ( $\Delta\phi_R$ ) versus  $\chi$  for two combinations of signaling state rate ( $k_F$ ) and ground state rate ( $k_R$ ), i.e., (a)  $(k_F, k_R) = (10^6, 10^6) s^{-1}$  (b)  $(k_F, k_R) = (10^6, 10^8) s^{-1}$  for five values of decoherence rate  $k$ . This result is for the two-nuclei based cryptochrome RP system ( $FAD_{1N}^{\bullet} - TrpH_{1N}^{\bullet}$ ) with  $D = 0$  and  $J = 0$ .

for  $(k_F, k_R) = (10^6, 10^6) s^{-1}$  and for  $(k_F, k_R) = (10^6, k_R = 10^8) s^{-1}$  in Fig. 10(b). Due to computational limitations, it was difficult to plot such a curve for the four-nuclei cryptochrome model. Instead, we use Eq. (7) and analyze the change in sensitivity due to CISS under various relaxation rates for a four-nuclei system. The two rate combinations considered were  $(k_F, k_R) = (10^6, 10^6) s^{-1}$  and  $(k_F, k_R) = (10^6, 10^8) s^{-1}$ . It has been summarized in Table III. The interesting point to note from this analysis is that  $\Delta M_S$  increase when relaxations rate increases for  $(k_F, k_R) = (10^6, 10^6) s^{-1}$  but decreases for  $(k_F, k_R) = (10^6, 10^8) s^{-1}$ . It must also be noted that the absolute value of sensitivity decreases as the relaxation rate increases for both  $\chi = 0$  and  $\chi = \frac{\pi}{2}$ . The ratio only highlights which case suffers more sensitivity deterioration due to relaxation. For example, at  $(k_F, k_R) = (10^6, 10^6) s^{-1}$  the drop in sensitivity is more for  $\chi = 0$  whereas for  $(k_F, k_R) = (10^6, 10^8) s^{-1}$ , the drop in sensitivity is more for  $\chi = \frac{\pi}{2}$ . At a high rate of decoherence,  $k = 10^7$ , we find that CISS provides a better sensitivity compared to no CISS case.

## V. CONCLUSION

In conclusion, we observe that the compass sensitivity is enhanced by the CISS effect for realistic recombination rate values. The functional window characteristic of the compass is, however, lost. We also observe that dipolar and exchange interaction are generally detrimental to the functioning of the avian compass, but it can be mitigated to a certain extent by CISS. We also observe that CISS supports compass sensitivity under environmental decoherence as well. In general, CISS

TABLE III.  $\Delta M_S$  for radical pair model based on four nuclei from cryptochrome molecule  $FAD_{2N}^{\bullet} - TrpH_{2N}^{\bullet}$  for various decoherence rate combinations at  $D = 0$  and  $J = 0$ .

Rate ( $s^{-1}$ )	$(k_F, k_R) = (10^6, 10^6) s^{-1}$	$(k_F, k_R) = (10^6, 10^8) s^{-1}$
$k = 0$	1.37	68.84
$k = 10^4$	1.39	66.35
$k = 10^5$	1.55	63.97
$k = 10^6$	4.27	57.31
$k = 10^7$	18.20	7.22

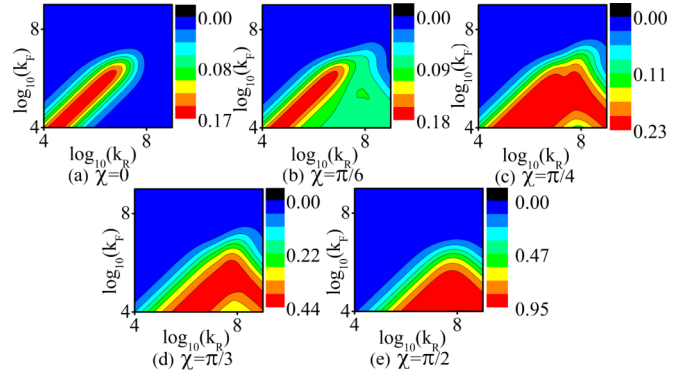


FIG. 11. Plots for sensitivity ( $\Delta\phi_R$ ) as a function of  $\log_{10}k_F$  and  $\log_{10}k_R$  for five distinct values of  $\chi$  showing varying degrees of spin selectivity due to CISS ( $0^\circ, 30^\circ, 45^\circ, 60^\circ, 90^\circ$ ) for the toy model.

seems to favor the RP model by enhancing its parameter regime to more realistic values. In future work, we plan to delve more deeply into the parameter regions where CISS is canceling the deleterious effects of dipolar and exchange interaction. We also plan to examine the RF disruption property of the avian compass in the presence of CISS. Finally, we would like to do this study on the full cryptochrome-based RP system that would require larger computational resources.

## ACKNOWLEDGMENTS

The author would like to thank Jiatae Luo and Peter J. Hore, Department of Chemistry, University of Oxford, UK, for an insightful communication about their work. This paper is supported by the Science and Engineering Research Board, Department of Science and Technology (DST), India, with Grants No. CRG/2021/007060 and No. DST/INSPIRE/04/2018/000023. The authors would also like to thank the Department of Electronics and Communication, IIT Roorkee, and the Ministry of Education, Government of India for supporting Y.T.'s graduate research.

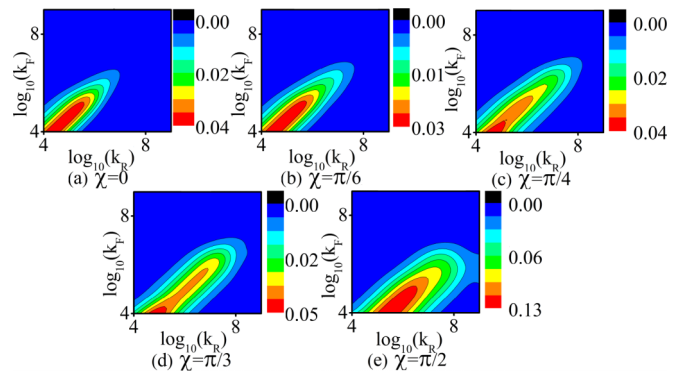


FIG. 12. Plots for sensitivity ( $\Delta\phi_R$ ) as a function of  $\log_{10}k_F$  and  $\log_{10}k_R$  for five distinct values of  $\chi$  showing varying degrees of spin selectivity due to CISS ( $0^\circ, 30^\circ, 45^\circ, 60^\circ, 90^\circ$ ) for the cryptochrome-based RP ( $FAD_{2N}^{\bullet} - TrpH_{2N}^{\bullet}$ ) system with four nuclei.

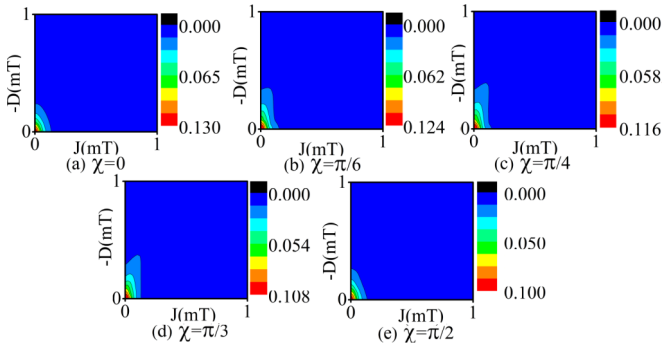


FIG. 13. Plots for sensitivity ( $\Delta\phi_R$ ) as a function of  $D$ (mT) and  $J$ (mT) for five distinct values of  $\chi$  showing varying degrees of spin selectivity due to CISS ( $0^\circ$ ,  $30^\circ$ ,  $45^\circ$ ,  $60^\circ$ ,  $90^\circ$ ) at  $(k_F, k_R) = (10^6, 10^6) s^{-1}$  for the toy model.

#### APPENDIX A: SENSITIVITY VERSUS RATES

We plot sensitivity for rate combination  $k_F, k_R \in [10^4, 10^9] s^{-1}$ , giving us a more holistic picture for the toy model and the four-nuclei cryptochrome system. We have plotted sensitivity  $\Delta\phi_R$  in Fig. 11 for the toy model and in Fig. 12 for the cryptochrome (four nuclei) RP system. This has been done for various values of rate  $k_F, k_R$  for five values of  $\chi$ . As observed in Fig. 2, we observe the similarity of sensitivity between the toy and cryptochrome (four nuclei) RP system. We observe in these plots that the maximum sensitivity  $\Delta\phi_R$  is attained at  $\chi = \frac{\pi}{2}$ . A major difference between the plots of sensitivity of toy and cryptochrome (four nuclei) molecules is the skewness of the area of maximum sensitivity. The rate combination of  $k_F, k_R$  for which we can derive increased sensitivity is far less for the cryptochrome (four nuclei) case than the toy model. Also, at  $\chi = \frac{\pi}{6}$ , we observe that the increase in sensitivity is very low for the toy model (with respect to  $\chi = 0$ , about 0.01), but it actually decreases for cryptochrome for a similar comparison. After analyzing Figs. 11 and 12, we observe that at high CISS, sensitivity is significant even at high rates of radical recombination. We observe that the protonation rate ( $k_F$ ) is a limiting factor in the RP model. If  $k_F$  is more than  $10^6 s^{-1}$ , the sensitivity becomes insignificant. An important point to note here is that the range of recombination rate to the ground state ( $k_R$ ) is increased in the presence of CISS. Thus CISS allows the RPM to have more realistic recombination rates (up to

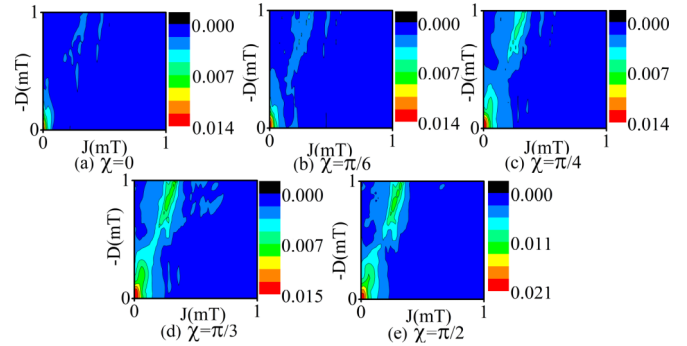


FIG. 14. Plots for sensitivity  $\Delta\phi_R$  as a function of  $D$ (mT) and  $J$ (mT) for five distinct values of  $\chi$  showing varying degrees of spin selectivity due to CISS ( $0^\circ$ ,  $30^\circ$ ,  $45^\circ$ ,  $60^\circ$ ,  $90^\circ$ ) at  $(k_F, k_R) = (10^6, 10^6) s^{-1}$  for four-nuclei  $FAD_{2N}^* - TrpH_{2N}^*$  based RP system.

$10^8 s^{-1}$ ). In a nutshell, we clearly demonstrate that CISS is increasing the sensitivity of the compass with more realistic recombination rates.

#### APPENDIX B: SENSITIVITY VERSUS DIPOLAR AND EXCHANGE INTERACTIONS

Figure 13 is the contour plot of sensitivity with respect to  $D$  and  $J$  for toy models at  $k_F = 10^6 s^{-1}, k_R = 10^6 s^{-1}$ . At  $D = 0$  and  $J = 0$ , we observe the maximum value of sensitivity, and it reduces if we move in any direction from that point. Here we observe that exchange and dipolar interaction have a maximum limit beyond which the sensitivity change is negligible. The dipolar interaction is limited at  $\sim \pm 0.4$  mT (for  $\chi = \frac{\pi}{4}$ ) and exchange interaction at  $\sim 0.1$  mT. We also observe that CISS affects this limit, but the change is insignificant. Figure 14 is the contour plot of sensitivity with respect to  $D$  and  $J$  for four nuclei taken from cryptochrome RPM at  $k_F = 10^6 s^{-1}, k_R = 10^6 s^{-1}$ . For  $\chi = 0$ , we observe that a higher value of dipolar interaction gives us some sensitivity for a finite value of  $J$ . This is in agreement with the result reported in Ref. [25], where partial cancellation of dipolar interaction occurs due to the finite value of exchange interaction. However, it is interesting to note that for  $\chi = \frac{\pi}{6}, \frac{\pi}{4}, \frac{\pi}{3}$ , and  $\frac{\pi}{2}$ , we observe that sensitivity increases manifold as well as the larger combination of  $J$  and  $D$  giving us sensitivity. Hence, this  $J/D$  cancellation increases as the system selectivity increases due to chirality.

- [1] J. L. Kirschvink, M. M. Walker, and C. E. Diebel, Magnetite-based magnetoreception, *Current opinion in neurobiology* **11**, 462 (2001).
- [2] G. Fleissner, B. Stahl, P. Thalau, G. Falkenberg, and G. Fleissner, A novel concept of fe-mineral-based magnetoreception: Histological and physicochemical data from the upper beak of homing pigeons, *Naturwissenschaften* **94**, 631 (2007).
- [3] T. Ritz, S. Adem, and K. Schulten, A model for photoreceptor-based magnetoreception in birds, *Biophys. J.* **78**, 707 (2000).
- [4] K. Schulten, C. E. Swenberg, and A. Weller, A biomagnetic sensory mechanism based on magnetic field modulated coherent electron spin motion, *Z. Phys. Chem.* **111**, 1 (1978).
- [5] P. J. Hore and H. Mouritsen, The radical-pair mechanism of magnetoreception, *Annu. Rev. Biophys.* **45**, 299 (2016).
- [6] M. Liedvogel, K. Maeda, K. Henbest, E. Schleicher, T. Simon, C. R. Timmel, P. Hore, and H. Mouritsen, Chemical magnetoreception: Bird cryptochrome 1a is excited by blue light and forms long-lived radical-pairs, *PLoS One* **2**, e1106 (2007).
- [7] K. Maeda, A. J. Robinson, K. B. Henbest, H. J. Hogben, T. Biskup, M. Ahmad, E. Schleicher, S. Weber, C. R. Timmel, and P. J. Hore, Magnetically sensitive light-induced reactions in cryptochrome are consistent with its proposed role as a magnetoreceptor, *Proc. Natl. Acad. Sci.* **109**, 4774 (2012).



- [8] B. D. Zoltowski, Y. Chelliah, A. Wickramaratne, L. Jarocha, N. Karki, W. Xu, H. Mouritsen, P. J. Hore, R. E. Hibbs, C. B. Green *et al.*, Chemical and structural analysis of a photoactive vertebrate cryptochrome from pigeon, *Proc. Natl. Acad. Sci.* **116**, 19449 (2019).
- [9] J. Xu, L. E. Jarocha, T. Zollitsch, M. Konowalczyk, K. B. Henbest, S. Richert, M. J. Golesworthy, J. Schmidt, V. Déjean, D. J. Sowood *et al.*, Magnetic sensitivity of cryptochrome 4 from a migratory songbird, *Nature (London)* **594**, 535 (2021).
- [10] J. Cai and M. B. Plenio, Chemical Compass Model for Avian Magnetoreception as a Quantum Coherent Device, *Phys. Rev. Lett.* **111**, 230503 (2013).
- [11] T. Baumgratz, M. Cramer, and M. B. Plenio, Quantifying Coherence, *Phys. Rev. Lett.* **113**, 140401 (2014).
- [12] K. Ray, S. Ananthavel, D. Waldeck, and R. Naaman, Asymmetric scattering of polarized electrons by organized organic films of chiral molecules, *Science* **283**, 814 (1999).
- [13] B. Göhler, V. Hamelbeck, T. Markus, M. Kettner, G. Hanne, Z. Vager, R. Naaman, and H. Zacharias, Spin selectivity in electron transmission through self-assembled monolayers of double-stranded DNA, *Science* **331**, 894 (2011).
- [14] R. Naaman and D. H. Waldeck, Chiral-induced spin selectivity effect, *J. Phys. Chem. Lett.* **3**, 2178 (2012).
- [15] R. Naaman and D. H. Waldeck, Spintronics and chirality: Spin selectivity in electron transport through chiral molecules, *Annu. Rev. Phys. Chem.* **66**, 263 (2015).
- [16] S. Dalum and P. Hedegård, Theory of chiral induced spin selectivity, *Nano Lett.* **19**, 5253 (2019).
- [17] K. Michaeli and R. Naaman, Origin of spin-dependent tunneling through chiral molecules, *J. Phys. Chem. C* **123**, 17043 (2019).
- [18] S. Matityahu, Y. Utsumi, A. Aharony, O. Entin-Wohlman, and C. A. Balseiro, Spin-dependent transport through a chiral molecule in the presence of spin-orbit interaction and nonunitary effects, *Phys. Rev. B* **93**, 075407 (2016).
- [19] J. Luo and P. Hore, Chiral-induced spin selectivity in the formation and recombination of radical pairs: Cryptochrome magnetoreception and EPR detection, *New J. Phys.* **23**, 043032 (2021).
- [20] W. Wiltschko and R. Wiltschko, Magnetic compass of European Robins, *Science* **176**, 62 (1972).
- [21] V. S. Poonia, K. Kondabagil, D. Saha, and S. Ganguly, Functional window of the avian compass, *Phys. Rev. E* **95**, 052417 (2017).
- [22] M. Winklhofer, E. Dylda, P. Thalau, W. Wiltschko, and R. Wiltschko, Avian magnetic compass can be tuned to anomalously low magnetic intensities, *Proc. R. Soc. London, Ser. B* **280**, 20130853 (2013).
- [23] C. Walcott, K. Schmidt-Koenig, and W. Keeton, Anomalies in the earth's magnetic field increase the scatter of pigeons' vanishing bearings, in *Animal Migration, Navigation and Homing*, edited by K. Schmidt-Koenig, and WT Keeton (1978), Vol. 143.
- [24] C. C. Finlay, S. Maus, C. D. Beggan, T. N. Bondar, A. Chambodut, T. A. Chernova, A. Chulliat, V. P. Golovkov, B. Hamilton, M. Hamoudi, R. Holme, G. Hulot, W. Kuang, B. Langlais, V. Lesur, F. J. Lowes, H. Lühr, S. Macmillan, M. Manda, S. McLean *et al.*, International Geomagnetic Reference Field: The eleventh generation, *Geophys. J. Int.* **183**, 1216 (2010).
- [25] O. Efimova and P. Hore, Role of exchange and dipolar interactions in the radical pair model of the avian magnetic compass, *Biophys. J.* **94**, 1565 (2008).
- [26] A. Einwich, P. K. Seth, R. Bartölke, P. Bolte, R. Feederle, K. Dedek, and H. Mouritsen, Localisation of cryptochrome 2 in the Avian retina, *J. Comp. Physiol. A* **208**, 69 (2022).
- [27] S. Y. Wong, Y. Wei, H. Mouritsen, I. A. Solov'yov, and P. Hore, Cryptochrome magnetoreception: Four tryptophans could be better than three, *J. R. Soc. Interface.* **18**, 20210601 (2021).
- [28] F. Cintolesi, T. Ritz, C. Kay, C. Timmel, and P. Hore, Anisotropic recombination of an immobilized photoinduced radical pair in a 50- $\mu$ t magnetic field: A model avian photomagnetoceptor, *Chem. Phys.* **294**, 385 (2003).
- [29] T. P. Fay, L. P. Lindoy, D. E. Manolopoulos, and P. Hore, How quantum is radical pair magnetoreception? *Faraday Discuss.* **221**, 77 (2020).
- [30] E. M. Gauger, E. Rieper, J. J. L. Morton, S. C. Benjamin, and V. Vedral, Sustained Quantum Coherence and Entanglement in the Avian Compass, *Phys. Rev. Lett.* **106**, 040503 (2011).
- [31] V. S. Poonia, D. Saha, and S. Ganguly, State transitions and decoherence in the avian compass, *Phys. Rev. E* **91**, 052709 (2015).
- [32] K. Schulten and P. G. Wolynes, Semiclassical description of electron spin motion in radicals including the effect of electron hopping, *J. Chem. Phys.* **68**, 3292 (1978).
- [33] H. Hiscock, Long-lived spin coherence in radical pair compass magnetoreception, Ph.D. thesis, University of Oxford, 2018.
- [34] G. Jeschke, Determination of the nanostructure of polymer materials by electron paramagnetic resonance spectroscopy, *Macromol. Rapid Commun.* **23**, 227 (2002).
- [35] A. R. O'Dea, A. F. Curtis, N. J. Green, C. R. Timmel, and P. Hore, Influence of dipolar interactions on radical pair recombination reactions subject to weak magnetic fields, *J. Phys. Chem. A* **109**, 869 (2005).